PCCP

Accepted Manuscript

ROYAL SOCIETY OF CHEMISTRY

rsc.li/pccp

View Article Online
DOI: 10.1039/C8CP02347F

PCCP

ARTICLE

Improvements in the hydrogen storage properties of the $Mg(NH_2)_2$-LiH composite by KOH addition

Received 00th January 20xx,
Accepted 00th January 20xx

DOI: 10.1039/x0xx00000x

www.rsc.org/

G. Amica*[a,b], S. Enzo[c], P. Arneodo Larochette[a,b], F. C. Gennari[a,b]

Potassium-containing compounds, such as KH, KOH, KNH_2 and different potassium halides, have shown positive effects on the dehydrogenation properties of the Li-Mg-N-H system. However, it is still discussed whether the K-compounds modify the thermodynamics of the system or if they have only a catalytic effect. In this work the impact of the addition of two K-containing compounds (0.08 mol% of KCl and KOH) in the hydrogen storage performance of the $Mg(NH_2)_2$-LiH composite was studied. The KOH incorporation reduced the dehydrogenation temperature from 197 °C to 154 °C, beginning the process at low temperature (~70 °C). The doped sample was able to reversibly absorb and desorb 4.6 wt% of hydrogen with improved kinetics: dehydrogenation rates were increased four times, whereas absorptions required 20% less time to be completed in comparison to the pristine material. The thermodynamic destabilization of the $Mg(NH_2)_2$-2LiH composite by the addition of a small amount of KOH was demonstrated by an increment of 30% in the dehydrogenation equilibrium pressure. According to detailed structural investigations, the KH formed by the KOH decomposition through milling and thermal treatment, can replace LiH and react with $Mg(NH_2)_2$ to produce a mixed potassium-lithium amide ($Li_3K(NH_2)_4$). The KH role is not limited to catalysis, but rather it is responsible for the thermodynamic destabilization of the $Mg(NH_2)_2$-LiH composite and it is actively involved in the dehydrogenation process.

1. Introduction

The hydrogen storage in light solid state medium is one of the most important challenges for the development of onboard applications. Since Chen et al. reported that Li_3N could reversibly store 11.4 wt% of hydrogen,[1] solid-state metal-N-H systems have been widely investigated and they have been considered as promising materials for safe and efficient hydrogen storage.[2-14] Among them, the $Mg(NH_2)_2$-LiH composite became one of the most attractive ones as approximately 5.5 wt% can be stored reversibly and its suitable thermodynamic parameters determine a desorption temperature lower than 100 °C at atmospheric pressure.[3,5] The hydrogen sorption pathway of this composite was proved to be a two-step reaction.[15]

$$2Mg(NH_2)_2 + 3LiH \rightarrow Li_2Mg_2(NH)_3 + LiNH_2 + 3H_2 \quad (1)$$

$$Li_2Mg_2(NH)_3 + LiNH_2 + LiH \rightarrow 2Li_2Mg(NH)_2 + H_2 \quad (2)$$

$$\text{In all: } 2Mg(NH_2)_2 + 4LiH \rightarrow 2Li_2Mg(NH)_2 + 4H_2 \quad 5.5 \text{ wt\% (3)}$$

However, due to its significant kinetic barrier, reasonable desorption rates are only achieved at temperatures over 200 °C.

The system kinetics could not be improved by the introduction of conventional catalysts, such as Ti, Fe, Co, Ni, Pd, Pt, and/or their chlorides. This is due to their lack of effectiveness in getting involved in the interfacial reactions and/or mass transport owing to poor solubility in amide, imide, or hydride.[16] Several factors such as atomic or ionic size, crystal structure, electronegativity and valence are important to determine the participation of the additive. Through partial replacement of LiH by KH, the set-off temperature for the potassium- modified system was remarkably reduced and ammonia emission was hardly detectable up to 200 °C.[16] Then, introducing an alkali metal dopant like potassium could be a strategy to enhance the dehydrogenation of the $Mg(NH_2)_2$ - LiH composite. As potassium can diffuse into the amide phase and combine with nitrogen, it was expected that the Li-N-H bonds in the amide and imide respectively were weakened. Moreover, there was evidence that potassium could form different ternary amides with magnesium or lithium.[17-23]

Since that moment, many investigations have been focused on the use of potassium-containing compounds to modify the $Mg(NH_2)_2$-LiH composite. The incorporation of KH, KOH, KNH_2 and different potassium halides allowed to reduce the desorption temperature and to improve the reactions rates without deterioration of the storage capacity. However, as there are large differences in the proposed reaction mechanisms, the discussion about the role of these additives is still open. Moreover, there are some strong differences regarding whether the K-compounds modify the thermodynamics of the system or if its effect is only catalytic. In general, the participation of K-containing mixed amides or imides such as $Li_3K(NH_2)_4$, $K_2Mg(NH_2)_4$ or $KMg(NH)(NH_2)$ in the reaction pathway was associated with the thermodynamic modification of

[a] Consejo Nacional de Investigaciones Científicas y Técnicas (CONICET) and Centro Atómico Bariloche (CNEA), Av. Bustillo 9500, R8402AGP, S. C. de Bariloche, Río Negro, Argentina. E-mail: guillerminaamica@gmail.com; Fax: +54294 4445190; Tel: +54294 4445712.
[b] Instituto Balseiro, Universidad Nacional de Cuyo, Argentina.
[c] Department of Chemistry and Pharmacy, University of Sassari, INSTM, Via Vienna 2, Sassari, Italy.

Electronic Supplementary Information (ESI) available: See DOI: 10.1039/x0xx00000x

View Article Online
DOI: 10.1039/C8CP02347F

the Li-Mg-N-H system,[23-25] but sometimes their detection was a difficult issue.[26-28] Various factors such as the degree of contact and the microstructure might have a role in favoring or not the formation of these phases.

Among different potassium halides (KF, KCl, KBr and KI) added, only KF reacts with LiH trough a metathesis reaction to convert to KH and LiF,[22] leading to a synergic thermodynamic and kinetic destabilization in the hydrogen storage reaction of the $Mg(NH_2)_2$-2LiH composite. Regarding the KH incorporation, Lin et al.[26] explained that KH was effective to reduce the dehydrogenation temperature of the $Mg(NH_2)_2$-$LiNH_2$-4LiH composite, while the ammonia emission was avoided. Although the reaction pathway was not modified, the decomposition was explained to proceed via non-stoichiometric compounds, considered as novel intermediate phases. Then, a catalytic role was attributed to KH and no K-containing amides or imides were involved. In other investigation, Li et al.[18] proposed that adding KH catalytically decreased the activation energy of the first dehydrogenation step and, in contrast, reduced the enthalpy of desorption during the second dehydrogenation. In this last step, KH participated as a reactant, forming $Li_3K(NH_2)_4$ and thus, changing the reaction pathway.

The influence of potassium cation substitution into $LiNH_2$ on the hydrogen storage properties of the $LiNH_2$-LiH composite was also explored and it was determined that the $KLi_3(NH_2)_4$-4LiH composite exhibited a superior cycling stability compared to the $LiNH_2$-LiH composite.[29] It was demonstrated that the ternary amide $KLi_3(NH_2)_4$ is an important intermediate in the hydrogenation/ dehydrogenation of the K-doped Li-N-H systems and it is formed by reaction between $LiNH_2$ and KNH_2 or through a solid reaction of $LiNH_2$ and KH under mechanical milling or thermal treatment.[21] Moreover, other investigations linked the hydrogenation kinetics improvement in Li-N-H systems to cycling reactions due to species continuously recycled such as $KLi_3(NH_2)_4$[19] or KH[30] with superior reactivity to H_2 and NH_3 respectively, producing a ''pseudo-catalytic'' effect. In opposition, Luo et al. affirmed that KH acted catalytically and not thermodynamically based on the similarity of the ΔH values for both K-doped and un-doped materials.[20] No new amide or imide K- containing species were detected.

Some investigations explored the use of KOH to modify the Li-N-H[24] and the Li-Mg-N-H systems.[22] In the former case, the key role of KOH in decreasing the activation energy and, consequently, the dehydrogenation temperature, was proved. In fact detailed structural investigations determined that KOH reacts with LiH during milling to convert to KH, which is the responsible for the improvements. In the latter case, Liang et al. observed a 74 °C reduction of the operational temperature for the first desorption cycle in comparison to the pristine material and they presented evidence of the interaction between the KOH additive and the reactants $Mg(NH_2)_2$ and LiH during milling.

Recently, Liu et al. presented some insights into the dehydrogenation process of a K-containing $Mg(NH_2)_2$-2LiH system.[28] They determined that KOH reacted during ball milling with $Mg(NH_2)_2$ and LiH to produce MgO, KH and $Li_2K(NH_2)_3$. During the initial heating at temperatures below 120 °C, KH and $Li_2K(NH_2)_3$ reacted with $Mg(NH_2)_2$ and LiH to form MgNH, $LiNH_2$ and $Li_3K(NH_2)_4$ while hydrogen was released. At higher temperatures $Li_3K(NH_2)_4$ reacted with $LiNH_2$ and LiH to produce $Li_2Mg(NH)_2$ and H_2. They also proposed a parallel reaction between $Li_3K(NH_2)_4$, $Li_2Mg(NH)_3$ and LiH that also released hydrogen. Analogously, when NaOH was added to the $Mg(NH_2)_2$-2LiH composite, a similar interaction during milling was observed, as NaOH reacts with $Mg(NH_2)_2$ and LiH to form NaH, $LiNH_2$ and MgO but a reduction of only 36 °C in the dehydrogenation temperature with respect to the pristine sample was observed.[31] Poorer results were obtained by adding NaH, suggesting K-compounds are more effective.

However, the K-doping was not a solution if working at high temperatures. Li et al.[27] presented the high-temperature (over 200 °C) failure behavior of K-based additives on the Li-Mg-N-H system due to changes in the crystal structure of the product after dehydrogenation, the enlargement in the grain and particle sizes and the increase in the inhomogeneous degree of mixing. Thus, they explained that as the failure was phenomenological, the key was to limit the operational temperatures.

In our previous work, we demonstrated that lithium fast-ion conductors have positive effects on the hydrogen storage properties of the Li-Mg-N-H due to the reduction of kinetic barriers and the catalytic role of the additive was associated to the weakening of the N-H bond.[12] In this work we modified the $Mg(NH_2)_2$-2LiH system by adding two K-containing compounds (0.08 mol% of KCl and KOH). The effect of K addition on dehydrogenation kinetics and thermodynamic stability of the $Mg(NH_2)_2$-2LiH composite was evaluated at 200 °C. As it was previously presented, all the investigations that have explored the effect of potassium compounds as dopants into the Li-Mg-N-H system, utilized $Mg(NH_2)_2$ previously synthesized and this compound was afterward milled with LiH and the potassium chosen additive, for example KOH, under hydrogen pressure (~80 bar). It is important to highlight that our synthesis procedure is different. In our case, $LiNH_2$, MgH_2 and the potassium additive were ball milled all together in an argon atmosphere. A mixture of $Mg(NH_2)_2$ and LiH was obtained and an excess of unreacted $LiNH_2$ and MgH_2 was detected. As a consequence there is a competence of reactivity between the K-additive and MgH_2 or $LiNH_2$ at the beginning of the milling and then, the possibility of interaction between the additive and $Mg(NH_2)_2$ or LiH, whether during milling or heating. A positive interaction between the potassium compounds and the sample was expected. On the basis of the collected experimental information, a proposal of dehydrogenation pathway is described. The present study opens new opportunities for designing K-modified $Mg(NH_2)_2$–LiH composites as promissory candidates for hydrogen storage.

2. Experimental

2.1 Synthesis of the composites

The starting materials were commercial $LiNH_2$ (Aldrich, 95%), MgH_2 (Aldrich, 98%), KOH (Biopack, 90%) and KCl (Mallinckrodt, 99.9%).The samples were handled in a MBraunUnilab argon-filled glove box, with oxygen and moisture levels lower than 1 ppm because of their high reactivity with the air components. For all studies, high purity hydrogen (Linde, 99.999%) and argon (Linde, 99.999%) were used. The sample preparation was carried out by mechanical milling (MM) of 2$LiNH_2$-MgH_2 (LM), 2$LiNH_2$-MgH_2-0.08KCl (LMKCl) and 2$LiNH_2$-MgH_2-0.08KOH (LMKOH). The milling

View Article Online
DOI: 10.1039/C8CP02347F
Physical Chemistry Chemical Physics ARTICLE

was performed in a planetary ball mill (Fritsch Pulverisette 6) rotating at 500 rpm for 20 h, using a sequence of 15 min milling and 10 min pause, with a ball to powder mass ratio of 53:1. To improve the powders mixing and eliminate possible dead zones, the milling was stopped to open the jar and to mix manually the material after 1, 3, 5, 10 and 15 h.

2.2 Characterization of the composites

Structural, microstructural, thermal and hydrogen storage properties of the as-milled and as-cycled samples were studied using differential scanning calorimetry (DSC, TA 2910 calorimeter), X-ray powder diffraction (XRPD, PANalytical Empyrean), Fourier transform infrared spectroscopy (FTIR, Perkin Elmer Spectrum 400), SEM-FIB (Zeiss, Crossbeam 340), thermogravimetry (TG-HP50, TA Instruments) and Sieverts-type volumetric equipment.

Structural information of the samples was obtained by XRPD (Cu Kα radiation, graphite monochromator) and FTIR. XRPD data was collected under Ar atmosphere using a tightly sealed sample holder to prevent the reaction between samples and air. For the FTIR measurements, powders were pressed into pellets with dry KBr inside of the glove box, placed in a specially designed cell to prevent air contamination and the spectra was collected at room temperature in the 800 – 4000 cm^{-1} wavenumber range. Samples for SEM were prepared in an argon-glove box by dispersing a small amount of powder on a commercial carbon tape, protected with gold sputtering and transferred in the microscope minimizing the air exposition. The thermal behavior of the samples was studied by DSC with a heating ramp of 5 °C min^{-1} and argon flow rate of 122 ml min^{-1}. About, 4-6 mg of sample was loaded into aluminum capsules closed in a glove box. The weight change of the samples was measured under helium gas flow while heating at 5 °C min^{-1}, using the same type of aluminum capsules than that used for DSC measurements.

Pressure-composition isotherms (PCI) and hydrogen sorption kinetics were obtained using a modified Sieverts-type equipment, coupled with a mass flow controller. The sample was transferred in the glove box inside a stainless reactor which was connected to the Sieverts device.

To perform PCI measurements each sample was first thermal treated. The hydrogen was extracted in fixed batches and two different criteria were used to determine if the system reached the equilibrium condition: the comparison between the temporal variation of the pressure and a fixed value (1.10^{-6} kPa s^{-1}) or the arrival to a selected waiting time (3000 seconds). When any of these criteria is met, the system is considered to be in equilibrium and a data point in the PCI curve is saved.

For kinetic isothermal measurements, the samples were surmounted to a thermal treatment at 200 °C under 6.0 MPa of hydrogen for 30 min before the first dehydrogenation. This step is named as thermal treatment (TT). Dehydrogenation curves were obtained at 200 °C with hydrogen back pressure of 0.05 MPa. The rehydrogenation curves were measured at 200 °C at a constant hydrogen pressure of 6.0 MPa. For non-isothermal measurements, the samples were heated at ~5 °Cmin^{-1} from room temperature up to 200 °C at 0.1 MPa of hydrogen pressure. The amount of absorbed/desorbed hydrogen was determined with a relative error ± 5 %. The hydrogen contents reported are expressed as wt% with respect to the total mass of each mixture.

Desorption curves at 200 °C were measured using different samples and each one was stopped at variable hydrogen content to determine both, the nature and the proportion of the crystalline phases by Rietveld method employing MAUD (Materials Analysis using Diffraction).[32,33]

3. Results and discussions

3.1 Thermal behaviour of as milled $LiNH_2$-$MgH_2$with different K-based additives

The hydrogen desorption properties of samples LM, LMKCl and LMKOH were first evaluated by DSC. The obtained profiles for the three samples are presented in Figure 1. It is shown that the 0.08 mol addition of KCl did not cause major changes in the shape of the curve in comparison to the pristine LM sample. Although the main endothermic peak seems to be sharper, it raised at almost the same temperature (it was reduced only 5 °C), suggesting that the additive did not interact with the sample at these conditions during milling, nor during heating. These observations are in agreement with previous investigations in which the effect of different potassium halides (KF, KCl, KBr, KI) into the $Mg(NH_2)_2$-2LiH composite was studied.[22] Among them, only the KF-added sample exhibited superior hydrogen storage properties, whereas samples with KCl, KBr and KI did not introduce any change. The effectiveness was attributed to the metathesis reaction between LiH and KF to convert to KH and LiF. They explained that the newly formed KH worked as catalyst in the initial heating process due to favorable thermodynamics and it reacted as an active compound in further steps.

Conversely, the shape of the curve for the LMKOH sample is very dissimilar. The main event is reflected in a much wider peak with two distinguishable and prominent shoulders, one before and other after. In this case, the 43 °C shift of the main event towards lower temperatures is evident, from 197 °C to 154 °C.

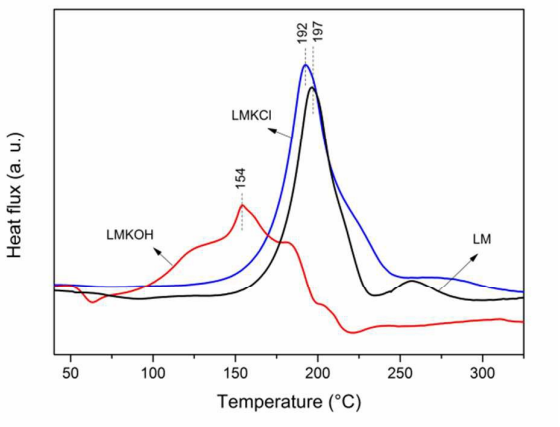

Figure 1: DSC profiles of the as-milled LM, LMKCl and LMKOH samples.

View Article Online
DOI: 10.1039/C8CP02347F

It is important to point out that the peak rise occurs at relatively low temperatures (~70 °C), which falls into the operating temperature range for PEMs. Moreover, the weak endothermic peak at 256 °C of sample LM disappears when adding a K-containing compound. The considerable modification of the curve and the shift towards lower temperatures suggest that the LMKOH system results much more interesting to explore.

3.2 Dehydrogenation kinetics of KOH doped composite

Thermogravimetric (Fig. 2A) and DSC (Fig. 2B) measurements were performed for the as-milled and the thermal treated samples, i.e. kept at 200 °C under a H_2 pressure of 6.0 MPa for 30 min. In both cases the curves seem to have two distinctive zones, one up to temperatures between 200-220 °C, having desorbed ~4 wt% of gas and another at higher temperatures. For the as-milled sample, the dehydrogenations begun at 110 °C, whereas after thermal treatment, the process was initiated over 150 °C. The small discrepancies in the values with respect to those observed by DSC (Fig. 1) are due to the dissimilar experimental arrangements which have their own fluid dynamics. Moreover, the differences between the MM and TT samples evidenced that the material changes its structure and / or microstructure when it was exposed to H_2 and temperature. This inevitable transformation occurs at the beginning of the cycling with hydrogen and then, it is the material which is worth to study.

To analyze the KOH effect on the hydrogen sorption behavior, volumetric measurements were carried out. Before the first dehydrogenation, the sample was thermally treated. Kinetics was distinctly improved and hydrogen release rates evidenced the beneficial utilization of potassium on the composite. The KOH doped sample was able to reversibly absorb and desorb 4.6 wt% of hydrogen at 200 °C (see Fig. 3).

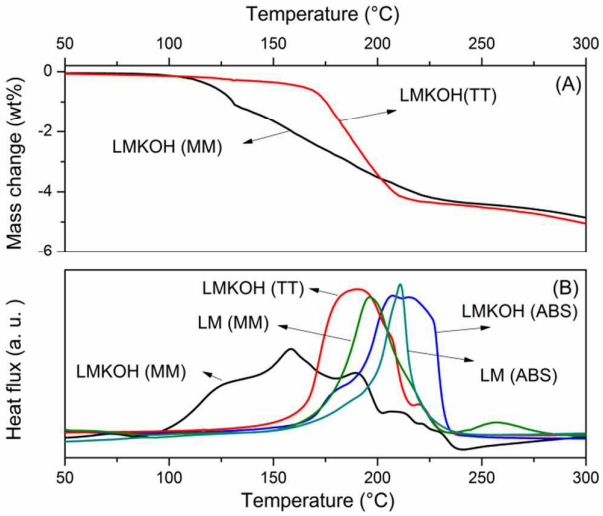

Figure 2: TG (A) and DSC measurements (B) for the MM and TT samples. In (B) the pristine LM (MM) and both LM and LMKOH samples absorbed after cycling are added. MM: mechanical milling; TT: thermal treatment; ABS: absorbed state.

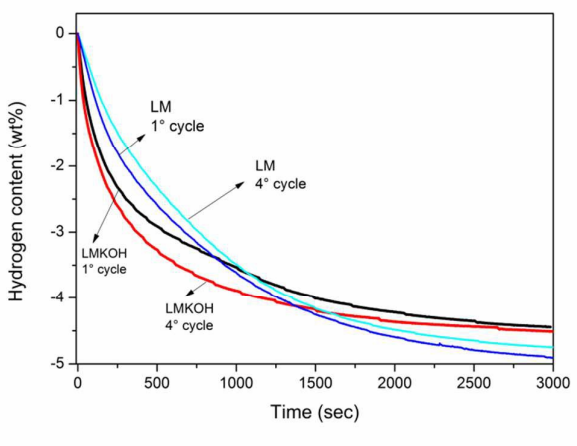

Figure 3: Desorption curves for samples LM and LMKOH at 200 °C (1° and 4° cycle).

Considering the slope between 0.02 wt% and 0.2 wt% of hydrogen released as a function of time for both samples, a dehydrogenation rate of 0.54 ± 0.05 wt% min^{-1} was obtained for the LM sample, in comparison to 2.35 ± 0.05 wt% min^{-1} for the 4th cycle of sample LMKOH. This shows that the dehydrogenation was four times faster due to the KOH addition. Sample LM needed almost 30 minutes to achieve 90% of its total capacity, whereas sample LMKOH required a 20% less. Despite the fact that the dehydrogenation temperature was slightly higher for the absorbed sample after cycling (Fig. 2B), consecutive volumetric measurements showed that kinetics at 200 °C were improved with cycling during the first cycles (Fig. 3). This is another evidence of the progressive compositional change of the material. On the other hand, the KOH addition during synthesis induces an experimental loss of approximately 5% of its capacity respect to LM.

3.3 Structural characterization of the ball milled and thermal treated samples

Structural characterization of the as-milled and thermal treated LMKOH samples was accomplished by XRPD and FTIR (see Fig. 4). Despite the fact that after milling the XRPD pattern showed a low crystallinity which disallowed to clearly identify any amides, crystalline MgH_2 and LiH were easily distinguished (Fig. 4B). This is due to the fact that after the milling a nanostructured material is obtained, with significant grain refinement.[6,26] The presence of amorphous KOH cannot be discarded because of the identification of broad peaks at 30.9 and 44.2°. It is important to point out that no other K-containing phases were identified, possibly due to lack of crystallinity. By FTIR, $Mg(NH_2)_2$ was unequivocally identified by its characteristic N-H vibrations at 3325 and 3271 cm^{-1} (Fig. 4A). This proves the interaction between $LiNH_2$ and MgH_2 during milling. The existence of residual $LiNH_2$ was demonstrated by its FTIR bands at 3313 and 3258 cm^{-1}. The crystallinity of the as-milled sample was improved after submitting it to thermal treatment at 200 °C under a hydrogen pressure of 6 MPa for 0.5 h. The nanostructure is destroyed as crystallite size of hydrides increases after temperature exposure.[6,26] The sample was mainly $Mg(NH_2)_2$, which was identified by XRPD and FTIR.

View Article Online
DOI: 10.1039/C8CP02347F
Physical Chemistry Chemical Physics ARTICLE

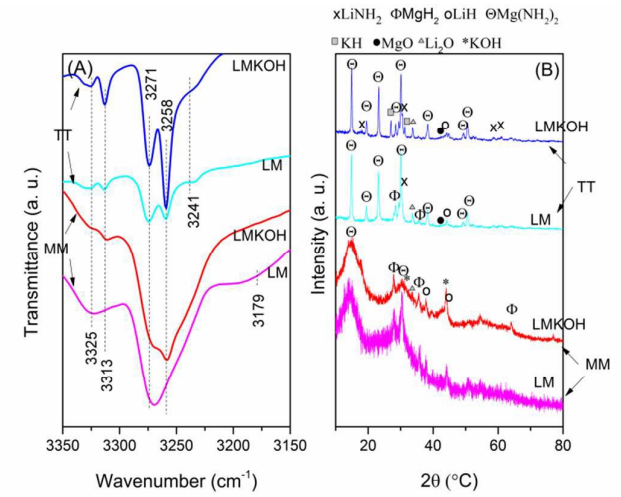

Fig. 4: FTIR (A) and XRPD (B) of samples LM and LMKOH after mechanical milling (MM) and thermal treatment (TT).

LiH was also distinguished. A little excess of $LiNH_2$ was detected but, differently from the milled sample, MgH_2 was not observed. The FTIR band at 3241 cm^{-1} has been previously reported as the decomposition products of $Li_2Mg(NH)_2$.[34] As no signs of KOH residues were observed by XRPD, the additive may have reacted completely during the heating. Instead, KH was clearly identified, as well as LiH and a small amount of MgO. This important change may be the responsible for the difference in the shapes of the curves detected by TG and DSC when the sample was submitted to temperature (Fig. 2). Moreover, at this point, there is no experimental evidence of the formation of mixed lithium potassium amides such as $Li_2K(NH_2)_3$ or $Li_3K(NH_2)_4$. Then, the main difference between both samples is the consumption of MgH_2, suggesting the $Mg(NH_2)_2$ formation by a reaction displacement, and the appearance of KH and MgO, possibly as a reaction product of the reaction with KOH. Then, the sample suffers both, structural and microstructural transformations due to temperature exposure, which may be the responsible for the dehydrogenation temperature increase. In Figure 4 the pristine LM sample (MM and TT) is also included for comparison. The LM sample after mechanical milling has a broad peak at 3179 cm^{-1} which can be associated with $Li_2Mg(NH)_2$. This band disappears after thermal treatment because of the complete hydrogenation while the band at 3241 cm^{-1} arises. As the band located at 3241 cm^{-1} is present for both, the pristine and the doped sample, it cannot be assigned to a K-containing phase. In spite of the accepted assignation of this band to the product of the decomposition of $Li_2Mg(NH)_2$,[34] recent investigations proposed that bands located at 3244 cm^{-1} and 3291 cm^{-1} could be attributed to lithium amide in a nonstoichiometric phase. This work presented Raman spectroscopy information about the nonstoichiometric continuum. It was explained that the peaks associated with the imide and amide groups in nonstoichiometric environments exhibited a linear shift in wavenumber with changes in the average stoichiometry.[35] A summary of the phases present in the samples is shown in Table 1.

Table 1: Species after mechanical milling and thermal treatment for the LM and LMKOH samples.

Sample	Mechanical milling		Thermal treatment	
	FTIR	XRPD	FTIR	XRPD
LM	$Mg(NH_2)_2$ $LiNH_2$ $Li_2Mg(NH)_2$	$Mg(NH_2)_2$ MgH_2 LiH	$Mg(NH_2)_2$ $LiNH_2$ Amide-imide groups in non-stoichiometric environments	$Mg(NH_2)_2$ $LiNH_2$ MgH_2 LiH
LMKOH	$Mg(NH_2)_2$ $LiNH_2$	$Mg(NH_2)_2$ MgH_2 LiH KOH Li_2O	$Mg(NH_2)_2$ $LiNH_2$ Amide-imide groups in non-stoichiometric environments	$Mg(NH_2)_2$ $LiNH_2$ MgO LiH KH

Microstructural information of the thermal treated sample was obtained by SEM analysis. Elemental mapping of the thermal treated sample allowed discarding any phenomenon of potassium segregation. In fact, K seemed to be homogeneously distributed, as well as Mg and N (see fig. 5). The presence of oxygen was detected in spite of the attempts to avoid air exposition.

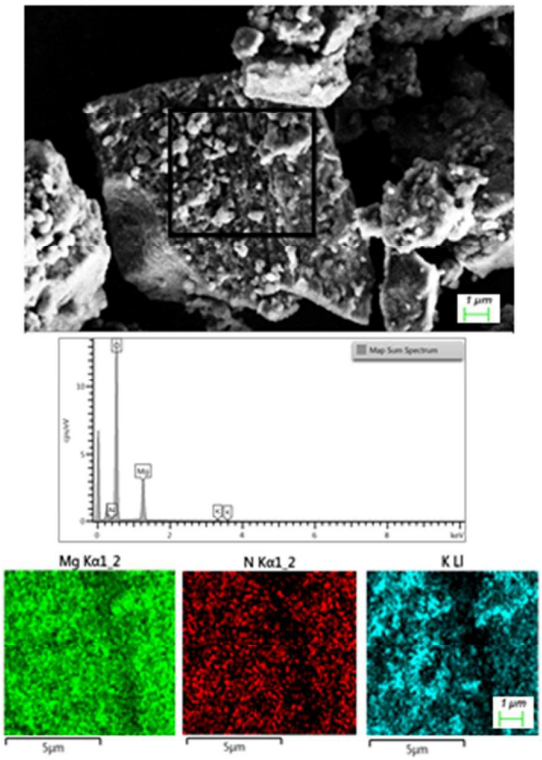

Figure 5: SEM micrographs, EDX spectrum and chemical mapping of the TT sample. The area analyzed is indicated in the secondary electron image.

View Article Online
DOI: 10.1039/C8CP02347F

In order to quantify the amount of each phase and determine the synthesis efficiency, Rietveld refinements were carried out for the thermal treated sample. Experimental and calculated data are shown in figure S1. The molar % and weight % of each phase is presented in table S1. Based on the amount of KOH added to the sample, it seems that there might be another K-containing phase in addition to the formed KH. As a distinguishable issue, for the LMKOH sample (TT), the phase molar ratio ($Mg(NH_2)_2/LiNH_2$) was approximately 60/40. Previous investigations in which the length of the thermal treatment was analyzed for the pristine sample LM, reported a molar relation of 59/41 for a 0.5 h treatment.[12] Then, the KOH addition did not contribute to the reaction displacement. For comparison, in these calculations only amides were considered, excluding LiH.

3.4 Structural characterization of dehydrogenated and hydrogenated samples

To analyze the role of the K compounds during hydrogen cycling, structural studies were performed on hydrogenated and dehydrogenated samples by FTIR and XRPD. For dehydrogenated samples, a structural comparison between two samples obtained following different procedures was realized: one sample was desorbed while heating (non- isothermally) and another one desorbed at a fixed temperature (isothermally). For the former, the milled sample was submitted to a non- isothermal dehydrogenation measurement, from room temperature up to 200 °C. Note that this procedure avoids the initial heating of the sample. It was shown that it started desorbing H_2 at 120 °C and the process was completed at 200 °C (Fig. S2). As regards the later, the sample was thermal treated and then exposed to desorption/absorption cycles at 200 °C, concluding with the sample in the desorbed state. There was no appreciable difference in the desorption capacities obtained by both procedures at 200 °C (~4.6 wt%) (Fig. 3 and S2).

FTIR analysis demonstrates that independently from the dehydrogenation process, both samples are similar (Fig. 6A). $LiNH_2$ was easily recognized by its characteristic bands at 3313 and 3258 cm^{-1}. The bands at 3297 $cm^{-1}$and 3258 cm^{-1} (the latter is overlapped with the band corresponding to $LiNH_2$) could be originated by the mixed potassium amide $Li_3K(NH_2)_4$.[28] As an observation, it can be said that these two bands were more pronounced for the non-isothermally dehydrogenated sample. The absorption peak centered at 3179 cm^{-1} was assigned to the cubic phase of the imide of composition $Li_2Mg(NH)_2$. There was no evidence of the presence of the intermediate imide phase $Li_2Mg_2(NH)_3$ (whose bands are located at 3198 and 3164 cm^{-1}). This means that the dehydrogenated doped samples do not present a mixture of $Li_2Mg(NH)_2$ and $Li_2Mg_2(NH)_3$ as it was observed for the pristine LM sample. Instead, the existence of Li-N-H nonstoichiometric phases could not be discarded because of the observance of the bands at 3291 cm^{-1} and 3244 cm^{-1}.[35] The XRPD pattern for the non-isothermally dehydrogenated sample seemed less crystalline (Fig. 6B). $Li_2Mg(NH)_2$, MgO, KH were easily identified, as well as a small amount of MgH_2, which may react during the second cycle. Consistently with the FTIR results, there was no evidence of $Li_2Mg_2(NH)_3$. As regards the isothermally dehydrogenated sample, the pattern was very similar, though MgH_2 was not detected. A summary of the phases that are present in the fully desorbed samples are shown in Table 2. The quantification of each phase was carried on by Rietveld refinements for isothermally dehydrogenated sample. Experimental and calculated data are shown in Table S2 and figure S3.

The absorbed state is unique and independent from the fact that the sample was desorbed isothermally or non-isothermally, achieving a sample stabilization. FTIR analyses (Fig. S4) proved the $Mg(NH_2)_2$ formation by the identification of its characteristic N-H vibrations at 3325 cm^{-1} and 3271 cm^{-1}, as well as $LiNH_2$ by its characteristic bands at 3313 cm^{-1} and 3258 cm^{-1}. No diffraction peaks of the $KLi_3(NH_2)_4$ phase was found which indicates that this phase may be active in the H_2 atmosphere at 200 °C.[19] As expected, by XRPD (Fig. S5) it was seen that the sample was mainly composed of $Mg(NH_2)_2$, $LiNH_2$ and LiH. KH and MgO were also detected. This means that the absorbed sample after hydrogen cycling is similar to the thermal treated one. Rietveld analysis was employed to determine the amount of each phase present in the absorbed sample. A small amount of Fe was detected which could be related to contamination with the milling chamber (see Table S3 and Fig. S5). Microstructural observation of the absorbed sample shows that after cycling with hydrogen, potassium seems to be less distributed and much localized in comparison with the thermal treated sample (see Fig. S6). This suggests that KH particles, the main K-containing phase in the hydrogenated state, trends to reorganize during hydrogen cycling.

Table 2: Species after isothermal and no isothermal dehydrogenation

Sample	Dehydrogenation ISO		Dehydrogenation NO ISO	
	FTIR	XRPD	FTIR	XRPD
LM	$LiNH_2$ $Li_2Mg_2(NH)_3$ $Li_2Mg(NH)_2$	$LiNH_2$ $Li_2Mg_2(NH)_3$ $Li_2Mg(NH)_2$ MgH_2	-	-
LMKOH	$LiNH_2$ $Li_2Mg(NH)_2$ $LiNH_2$ in nonstoi-chiometric state	$Li_2Mg(NH)_2$ $LiNH_2$ MgO KH	$LiNH_2$ $Li_2Mg(NH)_2$ $LiNH_2$ in nonstoi-chiometric state	$Li_2Mg(NH)_2$ $LiNH_2$ MgO KH MgH_2

View Article Online
DOI: 10.1039/C8CP02347F

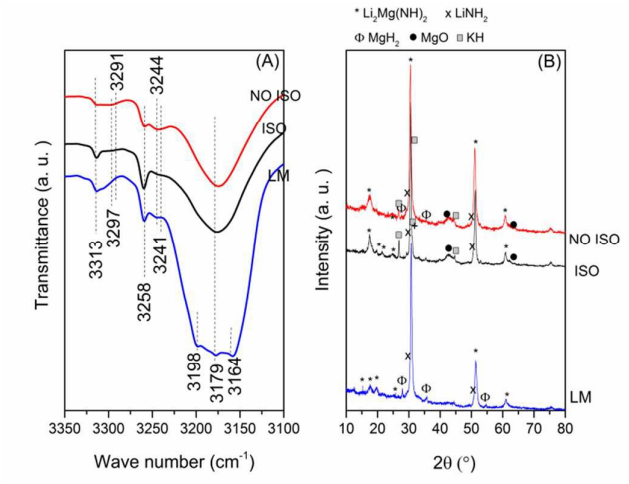

Figure 6: FTIR (A) and XRPD (B) of the desorbed LM sample and the isothermally and non-isothermally.

3.5 Thermodynamic analysis

In order to evaluate the thermodynamic stability of the KOH doped sample and compare it with the LM sample, pressure-composition isotherms of dehydrogenation were performed at 200 °C. The PCIs curves shown in Figure 7 were obtained using long waiting times for each point looking for equilibrium conditions (see section 2.2) and they both correspond to the third cycle of dehydrogenation, for the purpose of being independent from changes in the material during the first cycle. Cycling of PCIs at 200 °C of the LMKOH sample is presented in Figure S7. Sample LM evidenced a flat plateau of ~3.5 wt% at about 1.8 MPa of hydrogen pressure. As regards sample LMKOH, it showed a flat plateau too of ~2.7 wt% at about 2.4 MPa of hydrogen pressure. This notorious increase in the equilibrium pressure in more than 30 % is enough to assure the thermodynamic destabilization of the $Mg(NH_2)_2$-2LiH system by the addition of a small amount of KOH. The KH recognized in the structural characterization should be involved in the reaction mechanism to modify the equilibrium pressure.

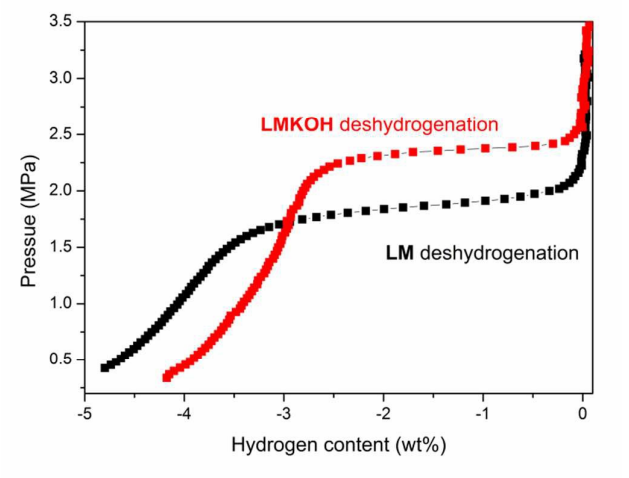

Figure 7: PCI of dehydrogenation at 200 °C for samples LM and LMKOH.

Moreover, the detection of the almost the same amount of KH in the dehydrogenated and hydrogenated states (see Table S3) suggest the existence of a cyclic mechanism of formation and consumption involving potassium as a participant.

3.6 Reaction pathways

With the aim of understanding the chemical transformations, several samples were collected at different points of the isothermal dehydrogenation (see Fig. 3). The desorption kinetic curve at 200 °C was measured using different samples and each one was stopped at variable hydrogen content. The samples collected (1, 2, 3 wt% and fully dehydrogenated) were studied by FTIR (Fig. 8) and XRPD (Fig. S8).

Through the whole process, $LiNH_2$ was easily recognized by its characteristic bands at 3313 and 3258 cm^{-1}. For all the desorbed samples a broad band in the area between 3200 and 3100 cm^{-1} was identified. The center of these broad bands shifted towards lower wavenumbers as dehydrogenation advanced as it is indicated in Fig. 8. When the dehydrogenation begun (1 wt%), it was centered at ~3193 cm^{-1}. As the process advanced (2 wt%), the intensity of the N-H vibrations of $Mg(NH_2)_2$ at 3325 and 3271 cm^{-1} became lower, indicating its gradual decomposition. Simultaneously there seemed to be a shift of the imide band towards the position ~3185 cm^{-1}. This is in agreement with XRD analyses (Fig. S8). When 3 wt% of hydrogen was released, practically all the $Mg(NH_2)_2$ was decomposed and the imide band centered at 3181 cm^{-1}. Moreover, the broad peak continued moving until the fully desorbed stage was achieved. At that point, the absorption peak centered at 3179 cm^{-1} was unequivocally assigned to the cubic phase of the imide $Li_2Mg(NH)_2$ and there was no longer any evidence about the presence of the intermediate imide phase $Li_2Mg_2(NH)_3$. The existence of a broad band in the imide zone, which was not perfectly centered at 3179 cm^{-1} suggested the mixture of the lithium magnesium imides: $Li_2Mg(NH)_2$ and $Li_2Mg_2(NH)_3$. The former is the final product of the dehydrogenation whereas the latter is in agreement with the decomposition of $Mg(NH_2)_2$ by a two-step reaction, through which $LiNH_2$ is also generated.

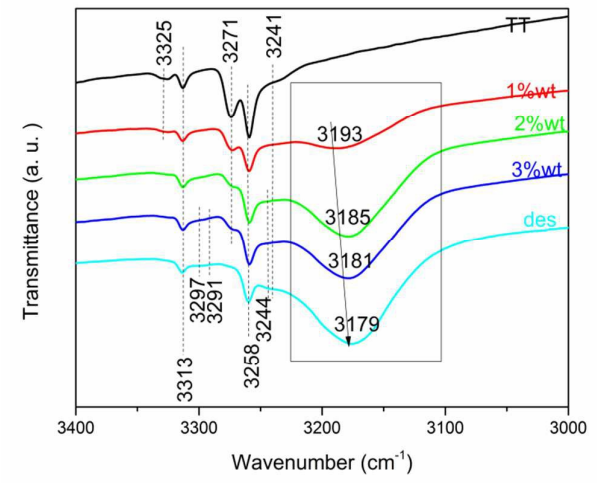

Figure 8: FTIR of samples at different stages of dehydrogenation of the LMKHOH sample.

View Article Online
DOI: 10.1039/C8CP02347F

The bands that belong to Li-N-H nonstoichiometric phases[35] at 3291 and 3244 cm^{-1} and the ones corresponding to $Li_3K(NH_2)_4$[28] at 3297 cm^{-1} and 3258 cm^{-1} are visible at the final steps of the dehydrogenation (3 wt% and fully desorbed). Unfortunately, the one located at 3258 cm^{-1} is overlapped with the band corresponding to $LiNH_2$. On the other hand, the identification of this mixed ternary potassium amide trough XRPD is not evident (Fig. S8). As it was previously reported, the low concentration and the peaks position adjacent to lithium and magnesium amides make the detection of the $Li_3K(NH_2)_4$ phase with FTIR and XRD very difficult.[28] The appearance of the $Li_3K(NH_2)_4$ phase by XRD has been reported at temperatures above 250 °C.[24]

Taking into account all the information recovered, the reaction pathway can be proposed as follows. During the mechanical milling and the sequential thermal treatment at 200 °C of the sample, reactions (4) and (5) occur and in total, reaction (6) is obtained.

$$2LiNH_2+MgH_2 \rightarrow Mg(NH_2)_2+2LiH \quad (4)$$

$$0.08Mg(NH_2)_2+0.16\,LiH+0.08KOH \rightarrow 0.08MgO+0.08KH+0.16LiNH_2 \quad (5)$$

$$\text{In total: } 2LiNH_2+MgH_2+0.08KOH \rightarrow 0.92Mg(NH_2)_2+0.08KH+1.84LiH+0.08H_2+0.08MgO+0.16LiNH_2 \quad (6)$$

Taking into account the quantities of each reactant, the beginning of the dehydrogenation can be described with reaction (7), which is catalysed by the KH newly formed. Then, the unreacted species can be listed: 0.08 MgO, 0.08 KH, 0.5LiH, 0.46 $Li_2Mg_2(NH)_3$ and 0.62 $LiNH_2$.

$$0.92Mg(NH_2)_2+1.38LiH \rightarrow 0.46Li_2Mg_2(NH)_3+0.46LiNH_2+1.38H_2 \quad (7)$$
Theoretical H_2 capacity: 3.9 wt%

The dehydrogenation process continues through reaction (8), in which KH is actively involved. The KH can replace the role of LiH as follows:

$$0.4LiNH_2+0.08Li_2Mg_2(NH)_3+0.08KH \rightarrow 0.16Li_2Mg(NH)_2+0.08Li_3K(NH_2)_4+0.08H_2 \quad (8)$$
Theoretical H_2 capacity: 0.2 wt%

Then, as the FTIR analysis results suggested, $Li_3K(NH_2)_4$ should be present in all the desorbed states. Even though this amide is hardly recognizable by XRPD. It was previously shown that the phase $Li_3K(NH_2)_4$ could not be identified after dehydrogenation at temperatures around 200 °C because of the occurrence of a metathesis reaction between $Li_3K(NH_2)_4$ and LiH to decompose into $LiNH_2$ and KH according to reaction (9).[29] As a consequence, there seems to be a cycle of formation and destruction which explains the change in the traditional reaction pathway of the potassium-doped composite and, as a consequence, upon thermodynamics.

$$Li_3K(NH_2)_4+LiH \rightarrow LiNH_2+KH \quad (9)$$

Moreover, independently from the occurrence of reaction (8), in which the potassium compound is involved, reaction (7) could also be followed by reaction (10):

$$0.46LiNH_2+0.46Li_2Mg_2(NH)_3+0.46LiH \rightarrow 0.92Li_2Mg(NH)_2+0.46H_2 \quad (10)$$
Theoretical H_2 capacity: 1.3 wt%

Reactions (8) and (10) compete but, together, they assure the quick dehydrogenation towards $Li_2Mg(NH)_2$ by consuming $Li_2Mg_2(NH)_3$ and $LiNH_2$. If reaction 8 occurs before reaction 10, then there is only an excess of $0.22LiNH_2$ available and instead of reaction (10), reaction (11) should be considered.

$$0.22LiNH_2+0.22Li_2Mg_2(NH)_3+0.22LiH \rightarrow 0.44Li_2Mg(NH)_2+0.22H_2 \quad (11)$$
Theoretical H_2 capacity: 0.6 wt%

The theoretical hydrogen capacities of all the reactions recently presented were calculated to respect to the initial mixture $2LiNH_2$-MgH_2, without considering KOH as a reactant. During ball milling, 0.11 wt% H_2 is lost irreversibly. The hydrogen generated during the dehydrogenation process is the sum of the produced by means of reactions (7), (8) and (11), which turned out to be 3.9, 0.2 and 0.6 wt% respectively. This means a total theoretical capacity of 4.7wt%. This result is in agreement within the experimental error with the observed hydrogen capacity during volumetric measurements (~4.6 wt%). Then, these three consecutive reactions together with reaction (9) constitute a cyclic mechanism that implies the formation and consumption of a potassium-containing, modifying the thermodynamics of the system with an improvement in dehydrogenation rate after hydrogen cycling.

Conclusions

The effect of two K-containing compounds (0.08 mol% of KCl and KOH) in the hydrogen storage performance of the $Mg(NH_2)_2$-LiH composite was studied in this work. The material was synthesized trough ball milling of $LiNH_2$ and MgH_2 with the potassium compound and a thermal treatment at 200 °C with 6.0 MPa H_2. The addition of KCl did not cause any reduction in the dehydrogenation temperature of the pristine material, suggesting that the additive did not interact with the other reactants during milling or heating. On the other hand, the KOH incorporation reduced the dehydrogenation temperature from 197 °C to 154 °C, beginning the process at low temperature (~70 °C).

Due to changes in both, its structure and microstructure, the dehydrogenation temperature of the LMKOH sample changed as it was exposed to H_2 and temperature.

Dehydrogenation behavior after successive cycles showed a beneficial effect of the KOH addition. The doped sample was able to reversibly absorb and desorb 4.6 wt% of hydrogen. Dehydrogenation rates were increased four times in comparison to the pristine material, whereas absorptions required 20% less time to be completed. Interestingly, consecutive volumetric measurements showed that kinetics were improved with cycling during the first cycles. A 30% increment in the dehydrogenation equilibrium pressure of the doped sample in comparison to the pristine one indicated the thermodynamic destabilization of the $Mg(NH_2)_2$-2LiH composite by the addition of a small amount of KOH. Based on the collected experimental information regarding structural characterization through XRPD and FTIR and taking into account the measured H_2 storage capacities, a proposal of dehydrogenation pathway involving the mixture of $Li_2Mg(NH)_2$ and

View Article Online
DOI: 10.1039/C8CP02347F
Physical Chemistry Chemical Physics ARTICLE

$Li_2Mg_2(NH)_3$ was presented. It was concluded that KOH reacted during milling to form MgO and KH. KH is actively involved in the reaction mechanism as it reacts during the dehydrogenation to produce a mixed potassium-lithium amide ($Li_3K(NH_2)_4$). Moreover, the detection of almost the same amount of KH in the dehydrogenated and hydrogenated states suggested the existence of a cyclic mechanism of formation and consumption, explaining the change in the traditional reaction pathway of the potassium-doped composite and upon thermodynamics.

Mixed potassium-lithium amides, such as $Li_3K(NH_2)_4$, were hardly detected by FTIR and XRD due to the low concentration and the overlap with peaks of lithium and magnesium amides. According to our results, the KH formed by the KOH decomposition is involved actively in the dehydrogenation process and participates in the formation of a compound which is responsible of the cyclic process that alter the reaction pathway.

Conflicts of interest

There are no conflicts to declare.

Acknowledgements

This study has been partially supported by CONICET (National Council of Scientific and Technological Research), CNEA (National Commission of Atomic Energy), ANPCyT (PICT N°1052) and Instituto Balseiro (University of Cuyo).

The authors would like to thank Alberto Baruj for the SEM images. F. C. Gennari gratefully acknowledges the financial support from L'Oréal-UNESCO National Award for Women in Science, in collaboration with CONICET (2016).

Notes and references

1 P. Chen, Z. Xiong, J. Luo, J. Lin and L. T. Tan, *Nature*, 2002, **420**, 302.
2 W. Luo, *J. Alloys Compd.*, 2004, **381**, 284.
3 Y. Nakamori, G. Kitahara and S. Orimo, J. *Power Sources*, 2004, **138**, 309.
4 Z. Xiong, G. Wu, J. J. Hu and P. Chen, *Adv. Mater.*, 2004, **16**,1522.
5 W. Luo and E. Rönnebro, *J. Alloy. Compd.*, 2005, **404-406**, 392.
6 F. C. Gennari, *Int. J. Hygrogen Energy*, 2011, **36**, 15231.
7 N. S. Gamba, P. Arneodo Larochette and F. Gennari, *RSC Advances*, 2015, **5**, 68542.
8 L. Fernandez Albanesi, P. Arneodo Larochette and F. C. Gennari, *Int. J. Hydrogen Energy*, 2013, **38**, 12325.
9 L. Fernandez Albanesi, S. Garroni, P. Arneodo Larochette, P. Nolis, G. Mulas, S. Enzo, M. D. Baró and F. Gennari, *Int. J. Hydrogen Energy*, 2015, **40**, 13506.
10 L. Fernandez Albanesi, S. Garroni, S. Enzo and F. C. Gennari, *Dalton Trans.*, 2016, **45**, 5808.
11 G. Amica, P. Arneodo Larochette and F. C. Gennari, *Int. J. Hydrogen Energy*, 2015, **40**, 9335.
12 G. Amica, F. Cova, P. Arneodo Larochette and F. C. Gennari, *Phys. Chem. Chem. Phys.*, 2016, **18**,17997.
13 H. Cao, Y. Zhang, J. Wang, Z. Xiong, G. Wu, P. Chen, *Progress in Natural Science: Materials International,* 2012, **22**, 550.
14 S. Garroni, A. Santoru, H. Cao, M. Dornheim, T. Klassen, C. Milanese, F. C. Gennari, C. Pistidda, *Energies*, 2018, **11**, 1027.
15 J. Hu, Y. Liu, G. Wu, Z. Xiong and P. Chen*, J. Phys. Chem. C*, 2007, **111**, 18439.
16 J. Wang, T. Liu, G. Wu, W. Li, Y. Liu, C. Moysés Araújo, R. H. Scheicher, A. Blomqvist, R. Ahuja, Z. Xiong, P. Yang, M. Gao, H. Pan and P. Chen, *Angew. Chem. Int. Ed.*, 2009, **48**, 5828.
17 J. Wang, G. Wu, Y. S. Chua, J. Guo, Z. Xiong, Y. Zhang, M. Gao, H. Pan, P. Chen, *Chem Sus Chem*, 2011, **4**, 1622.
18 C. Li, Y. Liu, Y. Pang, Y. Gu, M. Gao and H. Pan, *Dalton Trans.*, 2014, **43**, 2369.
19 B. Dong, Y. Teng, J. Ge, L. Song and S. Zhang, *RSC Advance*, 2013, **3**, 16977.
20 W. Luo, V. Stavila and L. E. Klebanof, *Int. J. Hydrogen Energy*, 2012, **27**,6646.
21 B. Dong, J. Gao, Y. Teng, H. Tian and L. Wang, *Int. J. Hydrogen Energy*, 2016, **41**, 5371.
22 Y. Liu, C. Li, B. Li, M. Gao and H. Pan, *J. Phys. Chem. C*, 2013, **117**, 866.
23 C. Liang, Y. Liu, M. Gao and H. Pan, *J. Mat. Chem. A*, 2013, **1**, 5031.
24 B. Dong, J. Ge, Y. Teng, J. Gao and L. Song, *J. Mat Chem A*, 2015, 3, 905.
25 A. Santoru, S. Garroni, C. Pistidda, C. Milanese, A. Girella, A. Marini, E. Masolo, A. Valentoni, N. Bergemann, T. Le, H. Cao, D. Haase, O. Balmes, K. Taube, G. Mulas, S. Enzo, E. Klassen and M. Dornheim, *Phys. Chem. Chem. Phys.*, 2016, **18**,3910.
26 H. Lin, H. Li, B. Paik, J. Wang and E. Akiba, *Dalton Trans*., 2016, **39**, 15374.
27 C. Li, Y. Liu, Y. Yang, M. Gao and H. Pan,*J. Mat. Chem. A*, 2014, 2, 7345.
28 Y. Liu, Y. Yang, X. Zhang, Y. Li, M. Gao and H. Pan, *Dalton Trans.*, 2015, **44**, 18012.
29 B. Dong, J. Gao, Y. Teng, H. Tian and L. Wang, *Int. J. Hydrogen Energy,* 2015, **41**, 5371.
30 Y. Teng, T. Ichikawa, H. Hiroki and Y. Kojima, *Chem. Comm.*, 2011, **47**, 12227.
31 C. Liang, Y. Liu, Z. Wei, Y. Jiang, F. Wu, M. Gao and H. Pan, *Int. J. Hydrogen Energy*, 2011, **36**, 2137.
32 Maud - Materials Analysis Using Diffraction, http://maud.radiographema.com/ (accessed January 2017).
33 L. Lutterotti, *Nucl. Inst. Methods Phys. Res. B*, 2010, **268**,334.
34 C. Liang, M. X. Gao, H. G. Pan and Y. F. Liu, *Appl. Phys. Let.*, 2014, **105**,0839609.
35 J. W. Makepeace and W. I. F. David, *The Journal of Physical Chemistry C*, 2017, **121**, 12010.